## Title
Foam film stratification studies probe intermicellar interactions



## Journal
Proceedings of the National Academy of Sciences of the United States of America, 118(25)

## ISSN
0027-8424

## Authors
Ochoa, Chrystian
Gao, Shang
Srivastava, Samanvaya
et al.

## Publication Date
2021-06-22

## DOI
10.1073/pnas.2024805118

Peer reviewed

# Foam film stratification studies probe intermicellar interactions

Chrystian Ochoa[a], Shang Gao[b], Samanvaya Srivastava[b,c,d,1], and Vivek Sharma[a,1]

[a]Department of Chemical Engineering, University of Illinois at Chicago, Chicago, IL 60608; [b]Department of Chemical and Biomolecular Engineering, University of California, Los Angeles, CA 90095; [c]California NanoSystems Institute, University of California, Los Angeles, CA 90095; and [d]Center for Biological Physics, University of California, Los Angeles, CA 90095

Edited by David A. Weitz, Harvard University, Cambridge, MA, and approved May 10, 2021 (received for review December 15, 2020)

**Ultrathin foam films containing supramolecular structures like micelles in bulk and adsorbed surfactant at the liquid–air interface undergo drainage via stratification. At a fixed surfactant concentration, the stepwise decrease in the average film thickness of a stratifying micellar film yields a characteristic step size that also describes the quantized thickness difference between coexisting thick–thin flat regions. Even though many published studies claim that step size equals intermicellar distance obtained using scattering from bulk solutions, we found no reports of a direct comparison between the two length scales. It is well established that step size is inversely proportional to the cubic root of surfactant concentration but cannot be estimated by adding micelle size to Debye length, as the latter is inversely proportional to the square root of surfactant concentration. In this contribution, we contrast the step size obtained from analysis of nanoscopic thickness variations and transitions in stratifying foam films using Interferometry Digital Imaging Optical Microscopy (IDIOM) protocols, that we developed, with the intermicellar distance obtained using small-angle X-ray scattering. We find that stratification driven by the confinement-induced layering of micelles within the liquid–air interfaces of a foam film provides a sensitive probe of non-DLVO (Derjaguin–Landau–Verwey–Overbeek) supramolecular oscillatory structural forces and micellar interactions.**

foams and emulsions | surface forces | X-ray scattering | soft matter | structural forces

Molecules in simple liquids and supramolecular structures in complex fluids can stratify or undergo confinement-induced layering induced by symmetry breaking at a solid–liquid or a fluid–fluid interface (1–8). In freestanding or foam films, the confinement-induced layering of supramolecular structures including micelles (9–17), lipid layers (18, 19), polyelectrolyte–surfactant complexes (20, 21), nanoparticles (9, 22), and liquid crystalline assemblies (23) can result in drainage via stratification. Due to thin film interference, foam films visualized under white light illumination display iridescent colors for thick films ($h > 100$ nm) (24–28), but ultrathin films ($h < 100$ nm) exhibit shades of gray that get progressively darker as the film gets thinner (9–21). In reflected light microscopy, micellar foam films exhibit coexisting thick–thin regions with distinct shades of gray. Interferometry-based measurement of the average film thickness over time decreases in a stepwise fashion yielding a step size, $\Delta h$ (9–17). Many published studies argue (9–12, 22, 29–34) that foam films containing charged micelles or latex particles stratify analogously due to the formation of "ordered colloidal crystals" (OCCs) and step size, $\Delta h$, equals the intermicellar distance, $d$, in bulk solutions. However, a comparison of concentration-dependent $\Delta h$ obtained from the dynamic foam stratification studies (influenced by confinement effects) with $d$ measured using small-angle X-ray or neutron scattering (SAXS or SANS) or other direct measurements of static equilibrium structure, and related evidence for or against the formation of OCCs in micellar foam films, are lacking in the literature. Thus, the motivations of this contribution are threefold: 1) contrast the step size, $\Delta h$, obtained via stratification studies with the intermicellar distance, $d$, and micelle dimensions determined using SAXS; 2) examine the SAXS data for any evidence of OCCs; and 3) elucidate the influence of ionic micelles on foam film stability and topography, as well as on colloidal forces, in multicomponent complex fluids.

Micelles, formed by self-assembly of soaps and detergents and ever present in typical household foams, facilitate cleaning and detergent action by solubilizing oils and oil-soluble dirt within their hydrophobic core (2, 34, 35). Micelles formed by biosurfactants like bile salt and rhamnolipids can be used for delivering nonpolar, bioactive polyunsaturated oils, flavonoids, vitamins, and hydrophobic drugs (36–38). Therefore, understanding the stability and lifetime of micellar foams is essential toward molecular engineering of formulations, controlling foams in industrial reactors, rivers, and lakes and developing bio-surfactants (36–38). Foam film drainage involves interfacial flows that are influenced both by bulk rheology and interfacial rheology as well as Laplace or capillary pressure, $P_c = \sigma C$ (set by surface tension, $\sigma$ and curvature, $C$) (27, 28, 39–41). Additionally, thickness transitions and variations in ultrathin ($h < 100$ nm) freestanding as well as supported (containing one or two solid boundaries) films (41–43) depend on disjoining pressure, $\Pi(h) = -(\partial G/\partial h)_{P,T,A,N_i}$, defined as the free energy required to change unit thickness at constant temperature, $T$, pressure, $P$, surface area, $A$, and mole number, $N_i$ (1, 34, 40–42). Intermolecular and surface forces determine the strength and range of disjoining pressure, $\Pi(h)$, as well as of colloidal interaction forces, $F(h)$ (1–3, 35, 40–42). Physical properties of surfactant solutions like surface tension and conductivity show distinct change around a critical micelle concentration (CMC), beyond

## Significance

Quantitative characterization of intermicellar distances and interactions requires the use of bespoke, expensive techniques like small angle X-ray or neutron scattering, surface force apparatus, and atomic force microscopy. Here, we utilize Interferometry Digital Imaging Optical Microscopy (IDIOM) protocols to characterize nanoscopic topographical changes and stepwise thinning in stratifying micellar foam films. We find that the step size equals the intermicellar distance obtained using small-angle X-ray scattering experiments on bulk solutions. Our direct comparison of these length-scales unequivocally supports the hydrodynamic mechanism for stratification based on thin-film equation and disjoining pressure computed using liquid-state theory. We envision that our contributions will inspire scientists to explore foam film studies as simple but effective methods for characterizing nanoscopic colloidal interactions and forces.

Author contributions: V.S. designed research; C.O., S.G., S.S., and V.S. performed research; C.O., S.G., S.S., and V.S. analyzed data; and C.O., S.G., S.S., and V.S. wrote the paper.

The authors declare no competing interest.

This article is a PNAS Direct Submission.



[1]To whom correspondence may be addressed. Email: samsri@ucla.edu or viveks@uic.edu.

This article contains supporting information online at https://www.pnas.org/lookup/suppl/doi:10.1073/pnas.2024805118/-/DCSupplemental.

Published June 16, 2021.

which spheroidal micelles can form (2, 34, 35), and rod-like micelles, lamellar phases, etc., emerge at higher concentrations (44–46). In foam films formed with ionic surfactant at $c < \text{CMC}$, drainage below $h < 30$ nm often leads to the formation of relatively long-lived common black (CB) film attributed to counterbalancing of $P_c$ by $\Pi_{DLVO}(h)$, the disjoining pressure due to DLVO (Derjaguin–Landau–Verwey–Overbeek) forces contributed by van der Waals and electrostatic double-layer interactions (1–3, 35, 39, 40). Even thinner Newton black (NB) films attest to the role of shorter-range, non-DLVO surface forces (14, 25–27, 40, 41). In contrast, in micellar foam films ($c > \text{CMC}$), a non-DLVO, oscillatory structural force, $\Pi_{OS}(h)$, counterbalances $P_c$ at multiple flat thicknesses, manifested as distinct shades of gray in reflected light microscopy (9–17, 21, 40, 47–50).

For micellar fluids containing charged micelles, the step size, $\Delta h$, obtained using thickness–time plots from stratification experiments, and periodicity, $\lambda$, of $\Pi_{OS}(h)$ directly measured using thin-film balance (47, 48) show that both periodicity and step size exceed micelle size, $a$, implying $\lambda > a$ and $\Delta h > a$. In 1971, Bruil and Lyklema (51) were the first to report that the concentration-dependent decrease in step size measured for sodium dodecyl sulfate (SDS) solutions followed a power law of the form $\Delta h \propto {c_{\text{soap}}}^{-1/3}$ and wrote that step size values "seem to be related to intermolecular distance in the (unmicellized) bulk solution." In 1988, Nikolov et al. (9) reported that foam films containing latex particles stratified in a fashion similar to micellar foam films and argued that diffusion-driven, layer-by-layer removal of micelles or particles from an ordered colloidal crystal (OCC) structure drives stratification. In their OCC or "micelle-vacancy diffusion" mechanism, they proposed that the effective film viscosity increases with decrease in stratified film thickness (9, 10, 29–31, 33). Contrastingly, in the "hydrodynamic" mechanism, Bergeron and Radke (13, 47) described stratification using a thin-film equation, by incorporating $\Pi_{OS}(h)$ and bulk solution viscosity. Nikolov et al. (9, 10, 29–31) suggested that the step size, $\Delta h$, was equal to an effective diameter, $d_{eff} = 2(l_{\text{SDS}} + \kappa^{-1})$, computed by adding the fixed length of SDS molecules, $l_{\text{SDS}}$, to the Debye length, $\kappa^{-1}$, that captures the range of screened electrostatic interactions. However, the step size $\Delta h \sim c^{-1/3}$ and the Debye length $\kappa^{-1} \sim c^{-1/2}$ display distinct power laws, and the measured step size exceeds the micelle size, $a$, as well as the computed effective diameter, $d_{eff}$, for ionic micellar systems, or typically $\Delta h > a$ and $\Delta h > d_{eff}$.

Studies on charged nanoparticle dispersions find that the periodicity, $\lambda$, of the oscillatory structural force, $F(h)$, measured directly with surface force apparatus (SFA), or colloidal probe atomic force microscopy (CP-AFM), correlates well with the interparticle distance, $d$, obtained using scattering and simulations (4, 5, 52–55). Furthermore, the periodicity, $\lambda \approx d \gg a$, is primarily set by the particle number density, $\rho$, and is relatively independent of added salt, charge at solid surfaces, and particle size, $a$ (4, 5, 53–55). Assuming that analogy between $\lambda \propto \rho^{-1/3}$ in the nanoparticle studies and $\Delta h \propto c^{-1/3}$ in stratified foam studies arises due to similar underlying physics, Danov et al. (32) and Anachkov et al. (11) argued that $\Delta h \approx d$ or step size equals the intermicellar distance, $d$, in bulk solutions and hypothesized that step size from stratification studies could be used for determining aggregation number as $N_{\text{agg}} \approx (c - \text{CMC})(\Delta h)^3$. However, Yilixiati et al. (17) showed that on salt addition, the measured $\Delta h$ values for micellar SDS solutions do not collapse onto a single curve even if plotted against micellar number density, $\rho$, as micelle number and dimensions can change on the addition of salt (or surfactant) (2), whereas nanoparticle dimensions remain constant. Furthermore, solid boundaries that can impact SFA and AFM measurements are absent in stratifying foam films. However, the thickness of stratifying films is rather heterogeneous, and the average thickness changes in a stepwise fashion. Thus, the analogy between stratifying micelles in foam films and stratifying nanoparticle dispersions under confinement between solid surfaces requires further investigation. In particular, a comparison between multiple length-scales including micelle dimensions, Debye length, intermicellar distance, $d$ and step-size, $\Delta h$, and the consequences of thickness heterogeneities within foam films are warranted.

In this study, we contrast the concentration-dependent changes in step-size measured in foam stratification studies with micellar dimensions and intermicellar distances in bulk solutions obtained using SAXS for aqueous solutions of SDS. For the range of concentrations (25 mM $\leq c_{\text{SDS}} \leq$ 250 mM) explored here, bulk rheology, interfacial tension, micelle shape and size, and interfacial charge (or potential) are nearly constant. Hence, the observed concentration-dependent changes in step-size and nanoscopic topography in stratifying films are dictated by the corresponding changes in intermicellar interactions and the resulting disjoining pressure, $\Pi_{OS}(h)$. We visualize and analyze nanoscopic thickness variations and transitions in stratifying foam films using IDIOM (Interferometry Digital Imaging Optical Microscopy) protocols (16) (Fig. 1*A*) that provide requisite spatiotemporal resolution (thickness ~1 nm, in-plane < 1 μm, time < 1 ms). We analyze SAXS data to compute micelle dimensions, volume fraction, and microstructure (order) in bulk solutions and obtain the intermicellar distance from structure factor peak in SAXS data. Finally, we discuss the ramifications of the close comparison between step size from the foam film stratification studies and micellar dimensions and intermicellar distance determined using SAXS analysis on the intermicellar interactions and the mechanistic basis of stratification.

## Results

**Drainage via Stepwise Thinning of Micellar SDS Foam Films.** The IDIOM setup, shown schematically in Fig. 1*A*, is utilized for visualization of a single foam film undergoing drainage and simultaneously for quantitative analysis of thickness variations and transitions (15–17, 48–50). A high-speed camera attached to a microscope captures the pixel-wise reflected light intensity that is determined by interference between light reflected from the two liquid–air interfaces of a single foam film, as sketched in Fig. 1*B*. The thickness of micellar foam films is obtained by analyzing average intensity from a square region (110 $\mu m^2$). Thickness decreases in stepwise fashion, as shown in Fig. 1*C*. The thickness profiles obtained for four distinct surfactant concentrations, shifted horizontally to aid clear visualization, feature two characteristic trends: the number of steps increases, whereas the step size decreases with an increase in surfactant concentration. For instance, the number of steps increases from 4 to 7, whereas the step size, $\Delta h$, decreases from $\Delta h = 13$ nm to $\Delta h = 7$ nm when SDS concentration is increased from 50 to 250 mM.

**Nanoscopic Topography of Stratifying Films, Characterized Using IDIOM Protocols.** Stratification in horizontal foam films visually manifests as shown in Fig. 2: regions with distinct thickness appear with contrasting shades of gray, and as thinner regions appear darker, the average thickness of the entire film decreases over time. Sharp contact lines demarcate the coexisting thick–thin regions, and the number of thinner, darker domains nucleated and observed decreases progressively. The concentration-dependent contrast in the number and duration of stepwise transitions and the topography of the films is highlighted in Fig. 2 (and in movies included as supplementary information). In addition to the snapshots that show the contrast in grayscale intensity, here we include representative thickness maps obtained by converting intensity into pixel-wise thickness using IDIOM protocols, as detailed elsewhere (16, 48, 49). Even though the measurements of step size are routinely carried out by using monochromatic light sources and photodiodes as detectors that measure the average reflected light intensity (27), the visualization and analysis of nanoscopic topographical features shown in Fig. 2 only began with the advent of IDIOM protocols (15–17, 48–50).

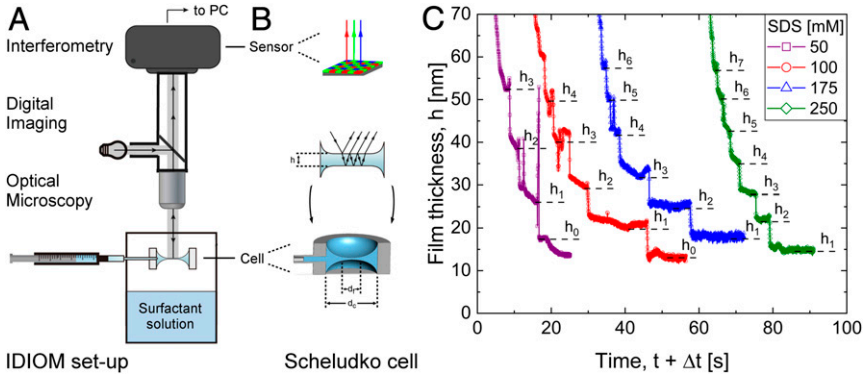


**Fig. 1.** Schematic of the setup used for examining stratification using IDIOM protocols and illustrative examples of stepwise thinning. (*A*) The Scheludko-like cell contains a plane-parallel film and surrounding meniscus that emulates a single foam film and its Plateau border. The cell is placed in a closed container and stratification is visualized using reflected light microscopy. A finite volume of fluid is inserted into the cell using the side-arm connected to a syringe. No liquid is added or withdrawn during the stratification experiment, and drainage from the film into the meniscus occurs freely and spontaneously. (*B*) Spatiotemporal variation in interference intensity $I(x, y, t; \lambda)$ is used for computing thickness transitions and variations in stratifying films. (*C*) Average film thickness plotted as a function of time shows stepwise thinning for foam films made with aqueous SDS solutions. The spikes and dips in thickness plots appear when mesas or domains emerge in the region selected for computing average thickness. The data are shifted horizontally for clarity.

The increase in the total number of flat regions that have distinct gray color and reflected light intensity values for the two concentrations included here (50 and 250 mM) are correlated with increase in the number of steps from 4 to 7 observed in Fig. 1*C*. The topographical maps reveal that in addition to flat regions (e.g., circular thinner, darker domains that spontaneously nucleate and grow during the stratification process), a spectrum of nonflat features including nanoridges and mesas also form and grow over time. For example, the necklace of bright, white spots observed in Fig. 2*H* turns out to be a chain of mesas in the corresponding thickness map whose the in-plane dimensions are in microns (see scale bar), and thickness is in nm (see colormap). Even though the hydrodynamic mechanisms predict the formation of nanoridge around a growing domain due to local volume conservation, the direct experimental evidence was lacking before Zhang and Sharma used IDIOM protocols and analysis based on thin-film equation to capture the shape evolution of nanoridges and nanoridge-to-mesa instability (15, 16, 48, 49). Zhang and Sharma (48) also showed that the nanoridge in the build-up region (going outwards from the thinner domain) exhibits a quasi-steady shape. In contrast, in the leeward region, the shape evolution is captured by a similarity solution, based on thin-film equation amended with an oscillatory structural disjoining pressure term, $\Pi_{OS}(h)$, with periodicity matched with step size. The topography observed here is dictated by the free drainage from the plane-parallel film into the meniscus that occurs under the influence of capillary pressure and is described in the creeping flow limit, avoiding the contributions of evaporation or Marangoni stresses on complex flows and fluxes associated with actively squeezed thin films, evaporating films, deformed films, and films with active withdrawal of the fluid (56–64).

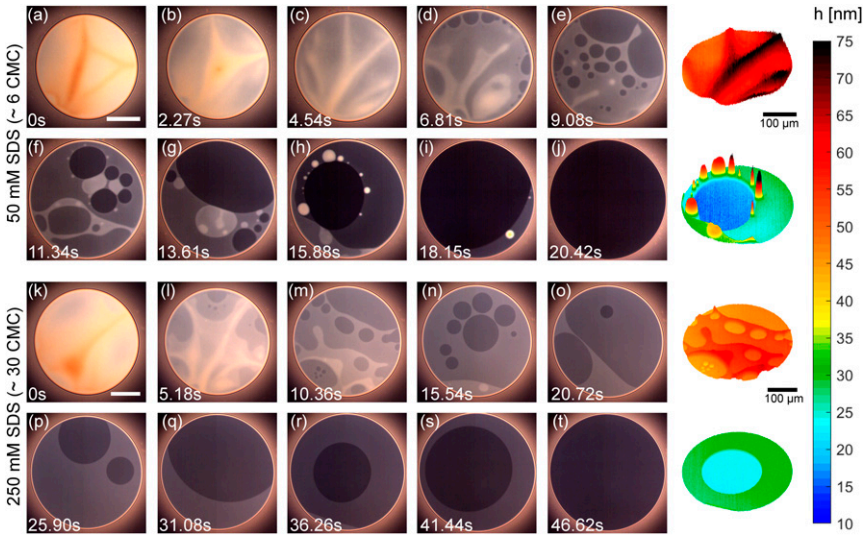


**Fig. 2.** Coexisting thick–thin regions in stratifying foam films made with 50 and 250 mM SDS solutions. The grayscale snapshots for 50 mM SDS data included in *A*–*J* and for 250 mM SDS in *K*–*T* obtained using reflected-light imaging, and the corresponding thickness maps based on four images (*C*, *H*, *M*, and *R*) are obtained using IDIOM protocols. The images were acquired in raw format to enable accurate determination of thickness maps (height is in nm, and the in-plane dimensions are in microns). The brightness and contrast of the grayscale snapshots are enhanced in ImageJ to discern distinct thickness regions easily. The snapshots included here (and Movies S1 and S2) show that the film drainage involves nucleation, growth, and coalescence of thinner, darker domains, as well as the appearance of brighter, white spots. The thickness maps show that domains are thinner, flat regions, whereas white spots can be nonflat and are labeled as mesas. The number of domains nucleated decreases as the overall film thickness decreases (e.g., notice the contrast between images *M* and *R*).

**SAXS of Micellar SDS Solutions.** The background-subtracted one-dimensional SAXS data for the micellar solutions with SDS concentration, $c_{SDS}$, ranging from 25 mM $\leq c_{SDS} \leq$ 225 mM, are shown in Fig. 3*A*. The overall scattering intensity, $I(q)$, measured as a function of wave vector $q$, can be described as a product of a form factor, $P(q)$, a structure factor, $S(q)$, and the micelle volume fraction, $\phi$, such that $I(q) \propto \phi P(q)S(q)$. Micelle dimensions (shape and size) can be determined from form factor, $P(q)$, whereas an analysis of the structure factor, $S(q)$, reveals information about intermicellar interaction and correlations that depend on charge and micelle number density (65). For SDS micelles, the hydrophobic core has a lower electron density than water, while the shell comprising the hydrophilic group and counter ions possesses a higher electron density than water. The combined influence of $P(q)$, $S(q)$, and the scattering length density differences (between solvent and shell and between shell and core) create distinct peaks and valleys in the X-ray scattering profiles of SDS micelles in contrast with the neutron scattering profiles (66). An analysis of the features in $I(q)$ and their corresponding length scale ($\sim 1/q$) reveal that the $I(q)$ peaks in the range 1 nm$^{-1} < q <$ 3 nm$^{-1}$ emerge owing to the contribution of $P(q)$, whereas the peaks in the range 0.4 nm$^{-1} < q <$ 1 nm$^{-1}$ are the contribution of $S(q)$. Upon increasing SDS concentration, $P(q)$ peak shifts from $q = 2$ nm$^{-1}$ for $c_{SDS} = 25$ mM to $q = 1.7$ nm$^{-1}$ for $c_{SDS} = 60$ mM, signifying a marginal growth of micelle dimensions in solution. However, the $P(q)$ peak position remains nearly $c_{SDS}$ invariant at $q \approx 1.7$ nm$^{-1}$ upon further increasing $c_{SDS}$ up to 225 mM, denoting nearly concentration-independent micelle sizes. Concomitantly, the $S(q)$ peak that appears in the $q$ range 0.4 nm$^{-1} < q <$ 1 nm$^{-1}$ becomes increasingly prominent as $c_{SDS}$ increases due to the strengthening of intermicellar correlations with an increase in micellar number density, $\rho \propto \phi$. This $S(q)$ peak also shifts to higher $q$ with increasing $c_{SDS}$, implying that the intermicellar distance, $d$, decreases with concentration.

Fits to the scattering spectra, $I(q) \sim \phi P(q)S(q)$ depicted in Fig. 3*A* with solid lines were obtained by combining a $P(q)$ model for oblate ellipsoidal core–shell micelles (67, 68) with a $S(q)$ model proposed by Hayter and Penfold (67, 69–71) based on the rescaled mean spherical approximation (RMSA) for particles interacting with screened Coulomb repulsion. The $P(q)$ fits reveal that SDS molecules self-assemble to form core–shell ellipsoids with the minor and the major axis radii $R_p \approx 1.3$ nm and $R_e \approx 2$ nm, respectively (an aspect ratio of $\approx$0.65), and a shell thickness $\approx$0.75 nm (see Fig. 3*B*), in good agreement with previous scattering studies on SDS micelles (46, 65, 66, 72, 73). The computed values of total charge ($Q < 30$ e$^-$) show that only a fraction of molecules is ionized. Micelle dimensions and computed charge are nearly independent of surfactant concentration for $c_{SDS} \geq 60$ mM. The micelle volume fraction, $\phi$, obtained from the structure factor fit, increases nearly linearly with $c_{SDS}$, as shown in Fig. 3*C*.

**Comparison between Step Size Obtained from Foam Stratification Studies and Intermicellar Distance Obtained from Scattering.** The structure factor, $S(q)$, extracted from the fits to $I(q)$ data shown in Fig. 4*A* for a range of SDS concentrations indicate that micelles are arranged in a disordered structure in bulk. The intermicellar correlations, correlated with the primary $S(q)$ peak amplitude, strengthen with increasing concentration. Estimates of intermicellar correlation distance, an indication of the average intermicellar distance, $d$, are obtained from the inverse of the position of the primary $S(q)$ peak, $q^*$, as $d = 2\pi/q^*$ (Fig. 4*A*). The magnitude of $q^*$ steadily increases with increasing $c_{SDS}$, denoting a decrease in correlation distance between micelles. The intermicellar distance, $d$, estimated from the primary $S(q)$ peaks, is found to be in excellent agreement with the step size, $\Delta h = h_{n+1} - h_n$, obtained from stratification experiments using IDIOM protocols, and both are found to display an inverse cubic root scaling $\Delta h \propto c_{SDS}^{-1/3}$ and $d \propto c_{SDS}^{-1/3}$ (denoted by dashed line), as shown in Fig. 4*B*. The agreement suggests that even though confining interfaces in thin films lead to layering of micelles, the interactions between micelles and their number density are not different from the bulk solution. The schematics illustrate how micelles distribute themselves self-consistently in bulk (Fig. 4*A*) and between interfaces under confinement (Fig. 4*B*) for micelles interacting pairwise with screened

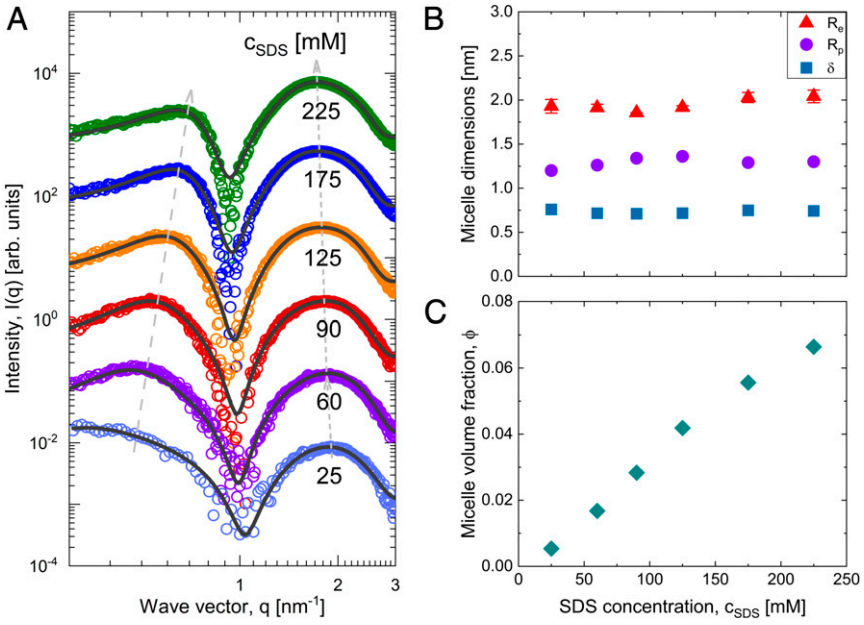


**Fig. 3.** SAXS results and micelle characteristics. (*A*) SAXS intensity patterns and the corresponding typical fits for aqueous SDS solutions with varying SDS concentrations. The fits use the form factor for oblate core–shell ellipsoids and the Hayter–Penfold structure factor, respectively. (*B*) Dimensions of the oblate SDS micelles: core radius along the major axis, $R_e$, and core radius along the minor axis, $R_p$, respectively, and shell thickness, $\delta$. (*C*) Micelle volume fraction, $\phi$, is rather low ($\phi < 0.1$) and is shown as a function of surfactant concentration, $c_{SDS}$.

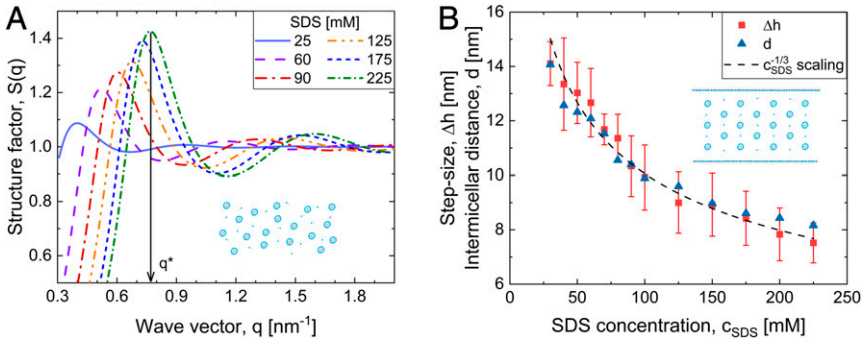


**Fig. 4.** Structure factor and concentration-dependent variation in step size and intermicellar distance. (*A*) Structure factor, $S(q)$, extracted using Hayter–Penfold model shows that the amplitude of the primary peak strengthens and peak position, $q^*$, shifts to higher $q$ with SDS concentration. (*B*) Step size obtained by analyzing stratification in micellar foam films using IDIOM protocols is compared to the intermicellar distance estimated from the inverse of the position of the primary ($q$) peak, $q^*$, as $2\pi/q^*$. The dashed line for −1/3 power law correlates well with the concentration-dependent change in step size and intermicellar distance. The schematics illustrate the distribution of micelles in bulk solution and in the thin film, respectively.

Coulomb interactions (are not drawn to scale). Despite these relatively low micelle volume fractions ($\phi < 0.1$), micelles, together with their Debye atmosphere, structure under confinement analogously to confined hard spheres of higher effective size and volume fraction (2, 3, 74–79). However, as the viscosity depends on the real size and volume fraction of micelles, the viscous resistance to drainage flows is not enhanced (4, 5, 76, 77).

## Discussion

The step size obtained from IDIOM protocols, shown in Fig. 4, shows reasonable agreement with the values obtained using conventional interferometry studies (16). Here, step size is reported for an extended range of concentrations (as high as 225 mM or $c$/CMC ~30). In contrast, most of the published studies were restricted to concentrations below 100 mM, except for three measurements, including a report by Krivchevsky and Stavans (78, 79) and the 1971 dataset from Bruil and Lyklema (51) that reported $\Delta h \propto {c_{soap}}^{-1/3}$. In the third dataset from 1984, Manev et al. (80) postulated that micellar SDS foam films stratify due to liquid crystallinity, following studies in the 1970s that found liquid crystal films display stratification (23, 81–84). However, there is no evidence for the formation of liquid crystals either in bulk solutions or in stratified films at low SDS concentrations investigated (including $c$/CMC < 5). Furthermore, for a fixed surfactant concentration, Manev et al. (80) reported that the step size varies during progressive thinning. In this study, the step size is relatively constant, consistent with the observations and analysis of Perrin (85, 86), Nikolov et al. (9, 10, 29), and other published literature (9–22, 29–34, 47–50, 85–90). Though the existence of two black films was well established by 1893 (91), Johonnott first reported the existence of multiple blacks (as many as five) in 1906 (90). After that, Perrin observed stepwise thinning with constant step size and cited stratification as evidence for molecular reality in his Nobel lecture in 1926 (85, 86). Even though the concepts underlying DLVO forces and the explanation for the two black films (NB and CB) emerged by the 1950s, a direct comparison between step size determined from stratification in micellar foam films and micellar dimensions and interactions remained unexplored before this study. Here, we discuss the import of our contributions on the longstanding debate between two mechanisms advanced for describing the thermodynamic and hydrodynamic phenomena that drive stratification in micellar foam films: 1) Stepwise thinning due to layer-by-layer removal of micelles from an OCC structure, with formation and growth of thinner, darker domains driven by diffusion of micelles and vacancies ("micelle-vacancy diffusion" or OCC mechanism), and increased viscosity of thinner films (9, 10, 29–31, 33); and 2) Stratification governed by thin-film equation, the "hydrodynamic" mechanism, wherein bulk viscosity describes fluid behavior, and nanoscopic topography manifests due to an interplay of disjoining pressure and capillary pressure.

In several papers, Nikolov, Wasan, Kralchevsky, and coworkers (9, 10, 29–31, 33) argued that ionic micelles undergo a phase transition to form OCC phases in analogy with the phase transitions reported by Hachishu et al. (92) for charged latex particles. Formation of ordered phases by highly charged spheres at relatively low volume fractions compared to hard spheres is observed in innumerable studies (93–97) with evidence from Bragg diffraction (92), scattering (95, 98, 99), microscopy [optical, total internal reflection, and confocal (99, 100)], among others. Since SDS micelles are relatively small, visualization of local microstructure using any optical microscopy techniques is ruled out, whereas SAXS facilitates investigation of the micelle arrangements and correlations. In contrast to the ordered phases observed in charged sphere suspensions, scattering spectra and the corresponding structure factors for SDS solutions obtained in our SAXS studies (Fig. 4*A*) do not show evidence of ordered colloidal ("micellar") crystals, and instead indicate disordered micelle arrangements with strengthening intermicellar correlations with increasing $c_{SDS}$. Previously published SAXS and SANS studies for SDS solutions (in the range of concentrations examined here) show a similar liquid-like structure comprising macroions (micelles) and their counterion cloud (70, 101–107).

Nikolov et al. (9, 10, 29–31, 33) assumed that interlayer spacing in films was less than the intermicellar distance in bulk and relied on the colloidal crystal picture to advance "micelle-vacancy diffusion" as a mechanism for stratification, arguing that domain expansion dynamics are governed by diffusion of micelles and vacancies. Furthermore, the cell model used by Nikolov et al. yields a series of disjoining pressures that arise due to the presence of certain layers of micelles rather than generating a single, oscillatory structural disjoining pressure. Bergeron and Radke (47) first measured the oscillatory structural disjoining pressure, $\Pi_{OS}(h)$, for SDS solutions and articulated that $\Pi_{OS}(h)$ is a continuous function of thickness. Bergeron and Radke (47) also showed that the step size obtained from thickness–time plots (dynamic measurement) is correlated with the periodicity, $\lambda$, measured for $\Pi_{OS}(h)$ or the supramolecular oscillatory force, measured using a thin-film balance (equilibrium measurement). In contrast with the OCC model, Bergeron, Jimenez-Laguna, and Radke (47) numerically solved the thin-film equation with oscillatory disjoining pressure term included to capture initial domain expansion dynamics and postulated that nonflat ridges form around growing domains due to mass conservation. Furthermore, Pollard and Radke (77) also showed via simulations that viscosity in micellar films is comparable to the bulk value (within 10%).

However, using the thin-film equation, Langevin and coworkers (89) argued that the domain expansion kinetics for stratifying films containing polyelectrolyte–surfactant complex is effectively determined by how quickly thickness changes diffuse away from a ridge, and inferred film viscosity was 60 times higher than bulk viscosity. Recently, Lee, Nikolov, and Wasan (12, 87, 88) reiterated the micelle vacancy-diffusion model and postulated that the viscosity of stratified films is itself thickness dependent and higher than bulk viscosity (nearly by an order of magnitude).

Even though the hydrodynamic models assume or predict that nanoridge forms around a growing domain, characterization and analysis of such nonflat structures began after the introduction of IDIOM protocols (15, 16, 48, 49). The "micelle-vacancy diffusion" or "colloidal crystal" mechanism does not explain the appearance of ridges, observed as brighter halos around growing domains in greyscale images obtained using reflected light microscopy, or in some instances, subsequent appearance of bright circular spots at moving front between expanding domain and its thicker surroundings, identified to be relatively flat, pancake-like structures we called mesas. Though Lee et al. (12) utilized the micelle-vacancy diffusion model to discuss domain expansion dynamics, they invoke Rayleigh instability to describe mesa formation, thus ignoring or contradicting their arguments about thickness-dependent viscosity and interaction energy, and the micelle-vacancy mechanism. Using IDIOM protocols and thin-film equation amended with disjoining pressure term, Zhang et al. (15, 16, 48, 49) recently showed that the size and shape evolution of nonflat regions including nanoridges and mesas is determined by the magnitude and periodicity of oscillatory structural contribution to disjoining pressure. The dynamics are indeed captured with the bulk viscosity values. Due to the presence of a thickness-dependent oscillatory disjoining pressure (or oscillatory free energy), the linear stability analysis predicts the possibility of a spinodal instability leading to the spontaneous emergence of mesh-like thick–thin regions driven purely by thin-film thermodynamics and hydrodynamics. Yilixiati et al. (50) showed that micellar foam films underwent such spinodal stratification and characterized the evolution of nanoscopic hills and gullies experimentally using IDIOM protocols. Thus, additional corroboration for the "hydrodynamic" mechanism can be attributed to the self-consistent explanation for domain expansion, nanoridge formation, nanoridge-to-mesa instability, and spinodal stratification (15–17, 48–50). However, as the hydrodynamic models involve a critical role for supramolecular oscillatory structural disjoining pressure contribution, we summarize the key progress made through the detailed studies of stratification.

Two non-DLVO, medium-mediated interactions arise in multicomponent colloidal dispersions due to structuring of smaller molecules, nanoparticles, micelles, or solvent molecules between larger, dispersed particles, bubbles, or drops: 1) depletion attraction caused by the depletion of smaller species from the confined region (8, 108–110) and 2) damped oscillatory structural disjoining pressure term, $\Pi_{OS}(h)$, contributed by layering in the confined region (4, 5, 21, 34, 40, 108–112). For simple fluids, Israelachvili, among others, proposed a phenomenological expression of the form $\Pi_{OS}(h) = A\exp(-h/\xi)\cos(2\pi h/\lambda + B)$, with periodicity, $\lambda$, and decay length, $\xi$, to describe damped oscillations (1–5, 8, 21, 42). For relatively short-ranged $\Pi_{OS}(h)$, called solvation forces, periodicity and decay length are both set by the molecular size, $\lambda = \xi = a$. Such forces can be directly measured using force-based techniques like SFA or CP-AFM (1–3). For micellar fluids containing ionic surfactants and charged micelles, the step size, $\Delta h$, obtained using thickness–time plots from the dynamic stratification experiments, and periodicity, $\lambda$, directly measured using thin-film balance under equilibrium conditions (47, 48) show $\Delta h = \lambda > a$ and $\xi > a$, implying that both periodicity (= step size) and decay length exceed micelle size. Using equilibrium density functional theory, Pollard and Radke (76) showed that oscillatory contribution to disjoining pressure could be computed numerically by treating micelles as hard spheres and interactions between them with screened-Coulomb Yukawa-type interactions.

Subsequently, Kralchevsky and Denkov used Henderson's theory for bidisperse colloids made up of hard spheres with large size difference to derive an analytical formula for $\Pi_{OS}(h)$ that depends on micelle number density and uses Carnahan–Starling compressibility factor computed using effective volume fraction (based on $d_{eff}$) (11, 32, 113). Yilixiati et al. (17) modified the phenomenological model by using step size for periodicity as well as an experimentally determined micelle number density and by computing compressibility factor for effective volume fraction based on $d_{eff} = 2(l_{SDS} + \kappa^{-1})$, such that $\kappa^{-1} = [8\pi l_B(\mathrm{CMC} + (\alpha/2)(c - \mathrm{CMC}))]^{-1/2}$, accounts for the influence of both concentration and degree of ionization, $\alpha$, of micelles. Here, $l_B$ is the Bjerrum length. Lastly, there are only a couple of experimental studies that attempt to characterize structure within micellar foam films directly, and these provide support for the intermicellar distance comparable to the step size. Krichevsky and Stavans (78, 79) used static and dynamic light scattering, in addition to reflectivity, and comparison with the bulk RMSA calculations to show that the micellar fluid behaves analogous to confined simple fluids, with a step size matched with intermicellar distance. Denkov et al. (114) found a lack of order in cryoelectron microscopy of vitrified micellar SDS foam films, even though latex particles formed nicely ordered arrays. Thus, the current state-of-the-art models for oscillatory structural contribution to disjoining pressure in foam films are based on liquid-state theory (8, 17, 34, 76, 113, 115), and these models provide a quantitative analysis of the hydrodynamic processes underlying stratification using thin-film equation (13, 15, 16, 48, 49).

The close comparison of intermicellar distance and micelle dimensions determined using scattering with step size measured in foam film stratification studies reveals that the micellar solutions can be considered as (disordered) liquids in the concentration range explored here. The corroboration from scattering datasets presented by Figs. 3 and 4 implies that screened Coulomb interactions that describe intermicellar interactions in bulk solutions play the defining role for stratifying, micellar foam films. The intermicellar distance and interactions present in foam films correlate with those in bulk solutions for aqueous SDS solutions. Thus, the comparison supports mechanistic description of stratification using hydrodynamic models that consider micellar solutions to be liquid like and incorporate confinement-induced layering via $\Pi_{OS}(h)$ term (13, 48, 49, 89). The thin-film equation amended with disjoining pressure provides a quantitative and self-consistent description of thickness transitions and variations observed with a high spatiotemporal resolution by IDIOM protocols (48–50) In the concentration regime explored here for SDS solutions, micelle dimensions, surface tension, interfacial charge, and rheology are all nearly matched. Hence, the stratification studies reveal the influence of amplitude and range of supramolecular oscillatory structural disjoining pressure and underlying intermicellar interactions. Therefore, a concentration-dependent increase in the number of steps, observed in Figs. 1 and 2, implies an increase in the magnitude of supramolecular oscillatory structural disjoining pressure. In contrast, a concentration-dependent decrease in step size can be correlated with the corresponding decrease in periodicity of $\Pi_{OS}(h)$. Analogous changes in the magnitude and the periodicity of oscillatory structural force, $F(h)$, are obtained from SFA or CP-AFM measurements for nanoparticle dispersions and micellar solutions (4, 5, 21, 52–55, 79, 107, 109).

## Conclusions

In this contribution, we utilize foam film stratification studies in combination with SAXS and address three longstanding, mechanistic questions about stratification. First, we show that the step size, $\Delta h$, obtained from foam film stratification studies is equal to the intermicellar distance, $d$, determined using SAXS. Step size

obtained from discrete jumps in average thickness versus time plots as well as from the difference in the thickness of flat regions are correlated with the periodicity of supramolecular oscillatory structural forces. Secondly, we find that the SAXS data does not provide any evidence for the formation of ordered colloidal crystals (OCCs). The microstructure can be described using Hayter–Penfold liquid-state theory based on the RMSA. We find that scattering datasets can be described using a model developed for scattering by a disordered suspension of charged spheres. The micelle dimensions (shape and size) remain nearly constant for the concentration range explored in this study. The comparison of scattering and stratification studies presented here suggests that the electrostatic interactions between ionic micelles give rise to structure in bulk solutions, and oscillatory structural disjoining pressure influence foam film stability and topography. The comparison also supports the mechanistic description of stratification using hydrodynamic models that consider micellar solutions to be liquid like and utilize the thin-film equation amended with disjoining pressure to quantitatively and self-consistently model thickness transitions and variations, observed with a high spatiotemporal resolution by IDIOM protocols. We anticipate that our results will facilitate the use of foam film stratification studies as a quick, frugal, and robust characterization of the strength and range of interactions between dispersed supramolecular structures, including micelles, macromolecules, and nanoparticles, especially in multicomponent complex fluids, and to provide insights into molecular engineering of formulations.

## Materials and Methods

**Drainage via Stratification Studies Using Scheludko-like Cell and IDIOM Protocols.** The setup, shown schematically in Fig. 1*A*, includes a Schedluko-like cell (39) to create a foam film of diameter 1 to 2 mm, with the surrounding thicker meniscus in contact with a glass or plastic tube emulating a Plateau border in contact with the plane-parallel film. The surfactant solutions were formulated with SDS (Sigma-Aldrich, L6026, purity > 99.0%) for 25 mM $\leq c_{SDS} \leq$ 250 mM in deionized water (resistivity of 18.2 MΩ · cm). CMC of 8.2 mM was obtained from maximum bubble pressure tensiometry and pendant drop tensiometry for these SDS solutions. The cell is placed in a closed container filled with aqueous surfactant solution to create a saturated atmosphere and minimize the influence of evaporation and air currents, which can influence drainage via stratification dynamics (25, 50). A biconcave drop is initially formed within the cell, and then the liquid is slowly withdrawn using a side arm connected to a syringe pump to create a plane-parallel film with desired size and initial thickness (< 100 nm). The drainage occurs under a constant volume and a constant Laplace pressure condition. The cell diameter, $d_c$, and plane-parallel film diameter, $d_f$, determine the Laplace pressure $P_c \approx 4\sigma d_c/(d_c^2 - d_f^2)$, in which $\sigma$ refers to the surface tension value (39). As the capillary pressure depends upon both the film size and the cell size, these sizes are kept similar for all stratification experiments to have a meaningful comparison (39).

The thin film is illuminated by white light from a Fiilex P360EX portable light-emitting diode light source, and a FASTCAM Mini UX100 high-speed camera attached to a magnification system (Navitar Zoom 6000 with an added microscope objective) is used for capturing intensity variations accompanying drainage in a single foam film. Every pixel in a color image obtained by a digital camera can be read as a composite of three intensities of red (wavelength $\lambda = 630$ nm), green ($\lambda = 546$ nm), and blue ($\lambda = 470$ nm) light. Each color channel has values in the range of 0 to 4,095 (for RAW image with 12-bit depth). The IDIOM protocols rely on white light illumination and use digital filtering to obtain simultaneous intensity maps for three wavelengths, as detailed elsewhere (15, 16) and consequently obtain thickness measurements by using the interferometry equation:

$$h = \left(\frac{\lambda}{2n\pi}\right)\arcsin\left(\sqrt{\frac{\Delta}{1 + 4R(1\text{-}\Delta)/(1-R)^2}}\right), \quad [1]$$

where $\lambda$ is the wavelength of light, $\Delta = (I - I_{min})/(I_{max} - I_{min})$ and $R = (n-1)^2/(n+1)^2$. Here, $I$ is the intensity value measured in each pixel, $I_{max}$ and $I_{min}$ are the maximum and minimum intensity values, and $n$ is the refractive index of the bulk solution. The Fresnel coefficient $R = (n-1)^2/(n+1)^2$ is computed by using the refractive index $n$ of the bulk solution [in this case, we assume $n = 1.33$ and hence thickness is an effective measurement (13, 15, 47)]. The image analysis is carried out in MATLAB R2020a with specially developed codes. Experiments are carried out at room temperature.

**SDS Intermicellar Distance and Micelle Dimensions Using SAXS.** SAXS measurements were performed at the Advanced Photon Source beamline 12-ID-B of Argonne National Laboratory. The solutions were placed in 2-mm thin-walled quartz capillary tubes (Charles Supper Company, Inc) and were equilibrated at room temperature for at least 24 h prior to the scattering experiments. The capillaries are placed in the linear path of 13 keV X-ray beam to obtain the scattering measurements. The one-dimensional scattering intensity, $I(q)$, was obtained from the azimuthal averaging of the two-dimensional scattering speckle data. Scattering from the solvent background was subtracted to obtain $I(q)$ from the SDS self-assemblies in the solution as a function of the wave vector $q = \frac{4\pi \sin\theta}{\lambda}$ ranging from 0.3 to 3 $nm^{-1}$. Here, $2\theta$ is the angle between the incident beam (and the sample) and the detector, and $\lambda$ is the wavelength of the radiation. As the intensity, $I(q)$, profile depends on the structure factor, $S(q)$, set by intermicellar interference effects and the form factor, $P(q)$, determined by intramicellar interference, the structural characteristics and the micellar charges are obtained by fitting the product $\phi P(q)S(q)$ to the experimental $I(q)$ data using custom-written scripts in MATLAB.

**Data Availability.** All study data are included in the article and/or supporting information.

**ACKNOWLEDGMENTS.** The SAXS measurements were performed and intensity data were collected at the X-ray Science Division beamline 12-ID-B at the Advanced Photon Source, Argonne National Laboratory. We acknowledge the support provided by Dr. Xiaobing Zuo. This research used the resources of the Advanced Photon Source, a US Department of Energy (DOE) Office of Science User Facility operated for the DOE Office of Science by Argonne National Laboratory under Contract No. DE-AC02-06CH11357. V.S. acknowledges funding support from NSF-CBET 1806011 (National Science Foundation–Chemical, Bioengineering, Environmental and Transport Systems) and the UIC College of Engineering. S.G. and S.S. acknowledge funding support from the UCLA Samueli School of Engineering and the Department of Chemical and Biomolecular Engineering. We acknowledge discussions with UIC ODESlab (optics dynamics elasticity and self-assembly laboratory at UIC) members, especially comments by Chenxian Xu, Lena Hassan, and Carina Martinez, previous studies by ODESlab alumni Dr. Yiran Zhang and Dr. Subinuer Yilixiati, and insightful feedback by Dr. Naveen Reddy (Hasselt University, Belgium).

1. B. V. Derjaguin, N. V. Churaev, V. M. Muller, *Surface Forces* (Springer, New York, 1987).
2. J. N. Israelachvili, *Intermolecular and Surface Forces* (Academic Press, ed. 3, 2011).
3. J. Israelachvili, M. Ruths, Brief history of intermolecular and intersurface forces in complex fluid systems. *Langmuir* **29**, 9605–9619 (2013).
4. M. Ludwig, M. U. Witt, R. von Klitzing, Bridging the gap between two different scaling laws for structuring of liquids under geometrical confinement. *Adv. Colloid Interface Sci.* **269**, 270–276 (2019).
5. M. Ludwig, R. von Klitzing, Progress in measurements of oscillatory forces and liquid properties under confinement. *Curr. Opin. Colloid Interface Sci.* **47**, 137–152 (2020).
6. P. Maroni *et al.*, Structuring of colloidal silica nanoparticle suspensions near water-silica interfaces probed by specular neutron reflectivity. *Phys. Chem. Chem. Phys.* **22**, 6449–6456 (2020).
7. F. Heslot, N. Fraysse, A. M. Cazabat, Molecular layering in the spreading of wetting liquid drops. *Nature* **338**, 640–642 (1989).
8. A. Trokhymchuk, D. Henderson, Depletion forces in bulk and in confined domains: From Asakura–Oosawa to recent statistical physics advances. *Curr. Opin. Colloid Interface Sci.* **20**, 32–38 (2015).
9. A. D. Nikolov, D. T. Wasan, P. A. Kralchevsky, I. B. Ivanov, "Ordered structures in thinning micellar foam and latex films" in *Ordering and Organisation in Ionic Solutions*, N. Ial. Sogami, Ed. (World Scientific, Singapore, 1988), pp. 302–414.
10. A. D. Nikolov, D. T. Wasan, Ordered micelle structuring in thin films formed from anionic surfactant solutions: I. Experimental. *J. Colloid Interface Sci.* **133**, 1–12 (1989).
11. S. E. Anachkov, K. D. Danov, E. S. Basheva, P. A. Kralchevsky, K. P. Ananthapadmanabhan, Determination of the aggregation number and charge of ionic surfactant micelles from the stepwise thinning of foam films. *Adv. Colloid Interface Sci.* **183-184**, 55–67 (2012).
12. J. Lee, A. Nikolov, D. Wasan, Stepwise thinning dynamics of a foam film formed from an anionic micellar solution. *J. Colloid Interface Sci.* **487**, 217–222 (2017).
13. V. Bergeron, A. I. Jimenez-Laguna, C. J. Radke, Hole formation and sheeting in the drainage of thin liquid films. *Langmuir* **8**, 3027–3032 (1992).
14. D. Langevin, A. A. Sonin, Thinning of soap films. *Adv. Colloid Interface Sci.* **51**, 1–27 (1994).
15. Y. Zhang, V. Sharma, Domain expansion dynamics in stratifying foam films: Experiments. *Soft Matter* **11**, 4408–4417 (2015).

16. Y. Zhang, S. Yilixiati, C. Pearsall, V. Sharma, Nanoscopic terraces, mesas, and ridges in freely standing thin films sculpted by supramolecular oscillatory surface forces. *ACS Nano* **10**, 4678–4683 (2016).
17. S. Yilixiati, R. Rafiq, Y. Zhang, V. Sharma, Influence of salt on supramolecular oscillatory structural forces and stratification in micellar freestanding films. *ACS Nano* **12**, 1050–1061 (2018).
18. Z. Lalchev, R. Todorov, D. Exerowa, Thin liquid films as a model to study surfactant layers on the alveolar surface. *Curr. Opin. Colloid Interface Sci.* **13**, 183–193 (2008).
19. P. J. Beltramo, J. Vermant, Simple optical imaging of nanoscale features in freeftanding films. *ACS Omega* **1**, 363–370 (2016).
20. C. M. Beltrán, D. Langevin, Stratification kinetics of polyelectrolyte solutions confined in thin films. *Phys. Rev. Lett.* **94**, 217803 (2005).
21. R. von Klitzing, E. Thormann, T. Nylander, D. Langevin, C. Stubenrauch, Confinement of linear polymers, surfactants, and particles between interfaces. *Adv. Colloid Interface Sci.* **155**, 19–31 (2010).
22. E. S. Basheva, K. D. Danov, P. A. Kralchevsky, Experimental study of particle structuring in vertical stratifying films from latex suspensions. *Langmuir* **13**, 4342–4348 (1997).
23. P. Oswald, P. Pieranski, *Smectic and Columnar Liquid Crystals: Concepts and Physical Properties Illustrated by Experiments* (CRC Press, 2005).
24. C. V. Boys, *Soap Bubbles: Their Colours and the Forces Which Mold Them* (Society for Promoting Christian Knowledge, London, 1912).
25. K. J. Mysels, S. Frankel, K. Shinoda, *Soap Films: Studies of their Thinning and a Bibliography* (Pergamon Press, 1959).
26. G. Gochev, D. Platikanov, R. Miller, Chronicles of foam films. *Adv. Colloid Interface Sci.* **233**, 115–125 (2016).
27. I. Cantat *et al*., *Foams: Structure and Dynamics* (Oxford University Press, 2013).
28. D. L. Weaire, S. Hutzler, *The Physics of Foams* (Oxford University Press, 1999).
29. A. D. Nikolov, P. A. Kralchevsky, I. B. Ivanov, D. T. Wasan, Ordered micelle structuring in thin films formed from anionic surfactant solutions: II. Model development. *J. Colloid Interface Sci.* **133**, 13–22 (1989).
30. P. A. Kralchevsky, A. D. Nikolov, D. T. Wasan, I. B. Ivanov, Formation and expansion of dark spots in stratifying foam films. *Langmuir* **6**, 1180–1189 (1990).
31. D. T. Wasan, A. D. Nikolov, P. A. Kralchevsky, I. B. Ivanov, Universality in film stratification due to colloid crystal formation. *Colloids Surf.* **67**, 139–145 (1992).
32. K. D. Danov, E. S. Basheva, P. A. Kralchevsky, K. P. Ananthapadmanabhan, A. Lips, The metastable states of foam films containing electrically charged micelles or particles: Experiment and quantitative interpretation. *Adv. Colloid Interface Sci.* **168**, 50–70 (2011).
33. D. T. Wasan, A. D. Nikolov, Thin liquid films containing micelles or nanoparticles. *Curr. Opin. Colloid Interface Sci.* **13**, 128–133 (2008).
34. P. A. Kralchevsky, K. D. Danov, N. D. Denkov, "Chemical physics of colloid systems and interfaces" in *Handbook of Surface and Colloid Chemistry*, K. S. Birdi, Ed. (CRC Press New York, ed. 2, 1997), vol. 2.
35. D. Fennell Evans, H. Wennerström, *The Colloidal Domain: Where Physics, Chemistry, Biology, and Technology Meet* (Wiley-VCH, New York, ed. 2, 1999).
36. A. Ferreira *et al*., Novel cosmetic formulations containing a biosurfactant from Lactobacillus paracasei. *Colloids Surf. B Biointerfaces* **155**, 522–529 (2017).
37. L. Bai, S. Huan, J. Gu, D. J. McClements, Fabrication of oil-in-water nanoemulsions by dual-channel microfluidization using natural emulsifiers: Saponins, phospholipids, proteins, and polysaccharides. *Food Hydrocoll.* **61**, 703–711 (2016).
38. X. Vecino, J. M. Cruz, A. B. Moldes, L. R. Rodrigues, Biosurfactants in cosmetic formulations: Trends and challenges. *Crit. Rev. Biotechnol.* **37**, 911–923 (2017).
39. A. Sheludko, Thin liquid films. *Adv. Colloid Interface Sci.* **1**, 391–464 (1967).
40. V. Bergeron, Forces and structure in thin liquid soap films. *J. Phys. Condens. Matter* **11**, R215–R238 (1999).
41. C. J. Radke, Film and membrane-model thermodynamics of free thin liquid films. *J. Colloid Interface Sci.* **449**, 462–479 (2015).
42. P. G. de Gennes, F. Brochard-Wyart, D. Quéré, *Capillarity and Wetting Phenomena: Drops, Bubbles, Pearls, Waves* (Springer-Verlag, New York, 2004).
43. S. Kalliadasis, U. Thiele, *Thin Films of Soft Matter* (SpringerWien NewYork, 2007).
44. V. Lutz-Bueno, M. Liebi, J. Kohlbrecher, P. Fischer, Intermicellar interactions and the viscoelasticity of surfactant solutions: Complementary use of SANS and SAXS. *Langmuir* **33**, 2617–2627 (2017).
45. C. C. A. Dreiss, Wormlike micelles: Where do we stand? Recent developments, linear rheology and scattering techniques. *Soft Matter* **3**, 956–970 (2007).
46. F. Reiss-Husson, V. Luzzati, The structure of the micellar solutions of some amphiphilic compounds in pure water as determined by absolute small-angle X-ray scattering techniques. *J. Phys. Chem.* **68**, 3504–3511 (1964).
47. V. Bergeron, C. J. Radke, Equilibrium measurements of oscillatory disjoining pressures in aqueous foam films. *Langmuir* **8**, 3020–3026 (1992).
48. Y. Zhang, V. Sharma, Nanoridge formation and dynamics of stratification in micellar freestanding films. *Langmuir* **34**, 1208–1217 (2018).
49. Y. Zhang, V. Sharma, Thickness-dependent phase transition drives nanoridge-to-mesa instability in micellar freestanding films. *Langmuir* **34**, 7922–7931 (2018).
50. S. Yilixiati, E. Wojcik, Y. Zhang, V. Sharma, Spinodal stratification in ultrathin micellar foam films. *MSDE* **4**, 626–638 (2019).
51. H. G. Bruil, J. Lyklema, Stratification in free liquid films. *Nat. Phys. Sci (Lond.)* **233**, 19–20 (1971).
52. S. H. L. Klapp, S. Grandner, Y. Zeng, R. von Klitzing, Asymptotic structure of charged colloids between two and three dimensions: The influence of salt. *J. Phys. Condens. Matter* **20**, (2008).
53. S. H. L. Klapp, S. Grandner, Y. Zeng, R. von Klitzing, Charged silica suspensions as model materials for liquids in confined geometries. *Soft Matter* **6**, 2330–2336 (2010).
54. Y. Zeng *et al*., Effect of particle size and Debye length on order parameters of colloidal silica suspensions under confinement. *Soft Matter* **7**, 10899–10909 (2011).
55. Y. Zeng, S. Schön, R. von Klitzing, Silica nanoparticle suspensions under confinement of thin liquid films. *J. Colloid Interface Sci.* **449**, 522–529 (2015).
56. E. Chatzigiannakis, J. Vermant, Breakup of thin liquid films: From stochastic to deterministic. *Phys. Rev. Lett.* **125**, 158001 (2020).
57. E. Chatzigiannakis, N. Jaensson, J. Vermant, Thin liquid films: Where hydrodynamics, capillarity, surface stresses, and intermolecular forces meet. *Curr. Opin. Colloid Interface Sci.* **53**, 101441 (2021).
58. V. Chandran Suja, M. Rodríguez-Hakim, J. Tajuelo, G. G. Fuller, Single bubble and drop techniques for characterizing foams and emulsions. *Adv. Colloid Interface Sci.* **286**, 102295 (2020).
59. V. Chandran Suja, A. Hadidi, A. Kannan, G. Fuller, Axisymmetry breaking, chaos, and symmetry recovery in bubble film thickness profiles due to evaporation-induced Marangoni flows. *Phys. Fluids* **33**, 012112 (2021).
60. E. Chevallier, A. Saint-Jalmes, I. Cantat, F. Lequeux, C. Monteux, Light induced flows opposing drainage in foams and thin-films using photosurfactants. *Soft Matter* **9**, 7054–7060 (2013).
61. V. Chandran Suja *et al*., Evaporation-induced foam stabilization in lubricating oils. *Proc. Natl. Acad. Sci. U.S.A.* **115**, 7919–7924 (2018).
62. A. Bussonnière, E. Shabalina, X. Ah-Thon, M. Le Fur, I. Cantat, Dynamical coupling between connected foam films: Interface transfer across the menisci. *Phys. Rev. Lett.* **124**, 018001 (2020).
63. L. Champougny *et al*., Influence of evaporation on soap film rupture. *Langmuir* **34**, 3221–3227 (2018).
64. S. Andrieux *et al*., Microfluidic thin film pressure balance for the study of complex thin films. *Lab Chip* **21**, 412–420 (2021).
65. B. Hammouda, Temperature effect on the nanostructure of SDS micelles in water. *J. Res. Natl. Inst. Stand. Technol.* **118**, 151–167 (2013).
66. S. L. Gawali *et al*., Discerning the structure factor of charged micelles in water and supercooled solvent by contrast variation X-ray scattering. *Langmuir* **35**, 9867–9877 (2019).
67. M. Kotlarchyk, S. H. Chen, Analysis of small angle neutron scattering spectra from polydisperse interacting colloids. *J. Chem. Phys.* **79**, 2461–2469 (1983).
68. S. S. Berr, Solvent isotope effects on alkytrimethylammonium bromide micelles as a function of alkyl chain length. *J. Phys. Chem.* **91**, 4760–4765 (1987).
69. J. B. Hayter, J. Penfold, An analytic structure factor for macroion solutions. *Mol. Phys.* **42**, 109–118 (1981).
70. J. B. Hayter, J. Penfold, Determination of micelle structure and charge by neutron small-angle scattering. *Colloid Polym. Sci.* **261**, 1022–1030 (1983).
71. J.-P. Hansen, J. B. Hayter, A rescaled MSA structure factor for dilute charged colloidal dispersions. *Mol. Phys.* **46**, 651–656 (1982).
72. K. Schäfer *et al*., Supramolecular packing drives morphological transitions of charged surfactant micelles. *Angew. Chem. Int. Ed. Engl.* **59**, 18591–18598 (2020).
73. G. V. Jensen, R. Lund, J. Gummel, T. Narayanan, J. S. Pedersen, Monitoring the transition from spherical to polymer-like surfactant micelles using small-angle X-ray scattering. *Angew. Chem. Int. Ed. Engl.* **53**, 11524–11528 (2014).
74. P. Tarazona, Free-energy density functional for hard spheres. *Phys. Rev. A Gen. Phys.* **31**, 2672–2679 (1985).
75. I. T. K. M. Bitsanis, T. K. Vanderlick, M. Tirrell, H. T. Davis, A tractable molecular theory of flow in strongly inhomogeneous fluids. *J. Chem. Phys.* **89**, 3152–3162 (1988).
76. M. L. Pollard, C. J. Radke, Density-functional modeling of structure and forces in thin micellar liquid films. *J. Chem. Phys.* **101**, 6979–6991 (1994).
77. M. L. Pollard, C. J. Radke, Effective viscosities in thin ionic micellar liquid films. *AIChE J.* **42**, 2005–2013 (1996).
78. O. Krichevsky, J. Stavans, Micellar stratification in soap films: A light scattering study. *Phys. Rev. Lett.* **74**, 2752–2755 (1995).
79. O. Krichevsky, J. Stavans, Confined fluid between two walls: The case of micelles inside a soap film. *Phys. Rev. E Stat. Phys. Plasmas Fluids Relat. Interdiscip. Topics* **55**, 7260 (1997).
80. E. D. Manev, S. V. Sazdanova, D. T. Wasan, Emulsion and foam stability - the effect of film size on film drainage. *J. Colloid Interface Sci.* **97**, 591–594 (1984).
81. S. Friberg, St. E. Linden, H. Saito, Thin films from liquid crystals. *Nature* **251**, 494 (1974).
82. C. Y. Young, R. Pindak, N. A. Clark, R. B. Meyer, Light-scattering study of two-dimensional molecular-orientation fluctuations in a freely suspended ferroelectric liquid-crystal film. *Phys. Rev. Lett.* **40**, 773 (1978).
83. E. B. Sirota, P. S. Pershan, L. B. Sorensen, J. Collett, X-ray and optical studies of the thickness dependence of the phase diagram of liquid-crystal films. *Phys. Rev. A Gen. Phys.* **36**, 2890–2901 (1987).
84. E. Manev, J. E. Proust, L. Ter-Minassian-Saraga, Structural disjoining pressure in thin films of liquid crystals. *Colloid Polym. Sci.* **255**, 1133–1135 (1977).
85. J. Perrin, La stratification des lames liquides. *Ann. Phys. (Paris)* **10**, 160–184 (1918).
86. J. Perrin, "Discontinuous Structure of Matter" in *Nobel Lectures, Physics 1922-1941* (Elsevier Publishing Company, Amsterdam, 1965).
87. J. Lee, A. Nikolov, D. Wasan, Stratification of a foam film formed from a nonionic micellar solution: Experiments and modeling. *Langmuir* **32**, 4837–4847 (2016).
88. J. Lee, A. Nikolov, D. Wasan, Stepwise dynamics of an anionic micellar film - formation of crown lenses. *J. Colloid Interface Sci.* **496**, 60–65 (2017).
89. P. Heinig, C. M. Beltrán, D. Langevin, Domain growth dynamics and local viscosity in stratifying foam films. *Phys. Rev. E Stat. Nonlin. Soft Matter Phys.* **73**, 051607 (2006).
90. E. S. Johonnott, LXVIII. The black spot in thin liquid films. *Philos. Mag.* **11**, 746–753 (1906).

91. A. W. Reinold, A. W. Rucker, On the thickness and electrical resistance of thin liquid films. *Proc. R. Soc. Lond.* **53**, 394–398 (1893).
92. S. Hachisu, Y. Kobayashi, A. Kose, Phase separation in monodisperse latexes. *J. Colloid Interface Sci.* **42**, 342–348 (1973).
93. M. O. Robbins, K. Kremer, G. S. Grest, Phase diagram and dynamics of Yukawa systems. *J. Chem. Phys.* **88**, 3286–3312 (1988).
94. P. Pieranski, Colloidal crystals. *Contemp. Phys.* **24**, 25–73 (1983).
95. Y. Monovoukas, A. P. Gast, The experimental phase diagram of charged colloidal suspensions. *J. Colloid Interface Sci.* **128**, 533–548 (1989).
96. C. A. Murray, D. G. Grier, Video microscopy of monodisperse colloidal systems. *Annu. Rev. Phys. Chem.* **47**, 421–462 (1996).
97. G. Nägele, On the dynamics and structure of charge-stabilized suspensions. *Phys. Rep.* **272**, 215–372 (1996).
98. E. B. Sirota *et al*., Complete phase diagram of a charged colloidal system: A synchrotron x-ray scattering study. *Phys. Rev. Lett.* **62**, 1524–1527 (1989).
99. H. Yoshida *et al*., Transitions between ordered and disordered phases and their coexistence in dilute ionic colloidal dispersions. *Langmuir* **15**, 2684–2702 (1999).
100. C. A. Murray, D. H. Van Winkle, Layering transitions in colloidal crystals as observed by diffraction and direct-lattice imaging. *Phys. Rev. A Gen. Phys.* **34**, 562–573 (1986).
101. R. Itri, L. Q. Amaral, Distance distribution function of sodium dodecyl sulfate micelles by x-ray scattering. *J. Phys. Chem.* **95**, 423–427 (1991).
102. A. T. Gubaidullin *et al*., Structure and dynamics of concentrated micellar solutions of sodium dodecyl sulfate. *Russ. Chem. Bull.* **65**, 158–166 (2016).
103. R. Itri, L. Q. Amaral, P. Mariani, Structure of the hexagonal phase of the sodium dodecyl sulfate and water system. *Phys. Rev. E Stat. Phys. Plasmas Fluids Relat. Interdiscip. Topics* **54**, 5211–5216 (1996).
104. B. Cabane, R. Duplessix, T. Zemb, High resolution neutron scattering on ionic surfactant micelles: SDS in water. *J. Phys. (Paris)* **46**, 2161–2178 (1985).
105. Y. Chevalier, T. Zemb, The structure of micelles and microemulsions. *Rep. Prog. Phys.* **53**, 279 (1990).
106. V. K. Aswal, P. S. Goyal, Counterions in the growth of ionic micelles in aqueous electrolyte solutions: A small-angle neutron scattering study. *Phys. Rev. E Stat. Phys. Plasmas Fluids Relat. Interdiscip. Topics* **61**, 2947 (2000).
107. R. F. Tabor *et al*., Structural forces in soft matter systems: Unique flocculation pathways between deformable droplets. *Soft Matter* **7**, 11334–11344 (2011).
108. R. Tuinier, H. N. W. Lekkerkerker, *Colloids and the Depletion Interaction* (Springer Netherlands, 2011).
109. G. K. James, J. Y. Walz, Experimental and theoretical investigation of the depletion and structural forces produced by ionic micelles. *Colloids Surf. A Physicochem. Eng. Asp.* **441**, 406–419 (2014).
110. M. Piech, J. Y. Walz, Direct measurement of depletion and structural forces in polydisperse, charged systems. *J. Colloid Interface Sci.* **253**, 117–129 (2002).
111. A. Sharma, J. Y. Walz, Direct measurement of the depletion interaction in a charged colloidal dispersion. *J. Chem. Soc., Faraday Trans.* **92**, 4997–5004 (1996).
112. A. Tulpar, P. R. Van Tassel, J. Y. Walz, Structuring of macroions confined between like-charged surfaces. *Langmuir* **22**, 2876–2883 (2006).
113. P. A. Kralchevsky, N. D. Denkov, Analytical expression for the oscillatory structural surface force. *Chem. Phys. Lett.* **240**, 385–392 (1995).
114. N. D. Denkov, H. Yoshimura, K. Nagayama, T. Kouyama, Nanoparticle arrays in freely suspended vitrified films. *Phys. Rev. Lett.* **76**, 2354–2357 (1996).
115. A. Trokhymchuk, D. Henderson, A. Nikolov, D. T. Wasan, Computer modeling of ionic micelle structuring in thin films. *J. Phys. Chem. B* **107**, 3927–3937 (2003).